Cross section of ^{3}He(^{3}He,$2p$)^{4}He measured at solar energies

M. Junker,[1,2] A. D'Alessandro,[1] S. Zavatarelli,[3] C. Arpesella,[1] E. Bellotti,[4] C. Broggini,[5] P. Corvisiero,[3] G. Fiorentini,[6] A. Fubini,[7] G. Gervino,[8] U. Greife,[2] C. Gustavino,[1] J. Lambert,[9] P. Prati,[3] W. S. Rodney,[9] C. Rolfs,[2] F. Strieder,[2] H. P. Trautvetter,[2] and D. Zahnow[2]

(The Luna Collaboration)

[1]*Laboratori Nazionali Gran Sasso, Assergi, Italy*
[2]*Institut für Experimentalphysik III, Ruhr-Universität Bochum, Germany*
[3]*Universitá di Genova, Dipartimento di Fisica and INFN, Genova, Italy*
[4]*Universitá di Milano, Dipartimento di Fisica and INFN, Milano, Italy*
[5]*INFN, Padova, Italy*
[6]*Universitá di Ferrara, Dipartimento di Fisica and INFN, Ferrara, Italy*
[7]*ENEA, Frascati and INFN, Torino, Italy*
[8]*Universitá di Torino, Dipartimento di Fisica Sperimentale and INFN, Torino, Italy*
[9]*Georgetown University, Washington, D.C. 20057-1002*

We report on the results of the ^{3}He(^{4}He,$2p$)^{4}He experiment at the underground accelerator facility LUNA (Gran Sasso). For the first time the lowest projectile energies utilized for the cross section measurement correspond to energies below the center of the solar Gamow peak ($E_0 = 22$ keV). The data provide no evidence for the existence of a hypothetical resonance in the energy range investigated. Although no extrapolation is needed anymore (except for energies at the low-energy tail of the Gamow peak), the data must be corrected for the effects of electron screening, clearly observed the first time for the ^{3}He(^{3}He,$2p$)^{4}He reaction. The effects are, however, larger than expected and not understood, leading presently to the largest uncertainty on the quoted $S_b(0)$ value for bare nuclides ($=5.40$ MeV b). [S0556-2813(98)04505-1]

PACS number(s): 26.65.+t, 25.90.+k

I. INTRODUCTION

Accurate knowledge of thermonuclear reaction rates is important [1,2] in understanding the generation of energy, the luminosity of neutrinos, and the synthesis of elements in stars. Due to the Coulomb barrier (height E_c) of the entrance channel, the reaction cross section $\sigma(E)$ drops nearly exponentially with decreasing energy E. Thus it becomes increasingly difficult to measure $\sigma(E)$ and to deduce the astrophysical $S(E)$ factor defined by the equation [2]

$$\sigma(E) = \frac{S(E)}{E} \exp(-2\pi\eta), \quad (1)$$

with the Sommerfeld parameter given by $2\pi\eta = 31.29 Z_1 Z_2 (\mu/E)^{1/2}$. The quantities Z_1 and Z_2 are the nuclear charges of the interacting particles in the entrance channel, μ is the reduced mass (in units of amu), and E is the center-of-mass energy (in units of keV). Although experimental techniques have improved [2] significantly over the years to extend $\sigma(E)$ measurements to lower energies, it has not yet been possible to measure $\sigma(E)$ within the thermal energy region in stars. This region is determined by the Gamow energy window $E_0 \pm \delta E_0$ (the Gamow peak) for a given stellar temperature and lies far below the height of the Coulomb barrier, approximately at $E_0/E_c = 0.01$. Instead, the observed $\sigma(E)$ data at higher energies had to be extrapolated to thermal energies. As always in physics, such an extrapolation into the unknown can lead to considerable uncertainties.

The low-energy studies of thermonuclear reactions in a laboratory at the Earth's surface are hampered predominantly by the effects of cosmic rays in the detectors. Passive shielding around the detectors provides a reduction of γ's and neutrons from the environment, but it produces at the same time an increase of γ's and neutrons due to the cosmic-ray interactions in the shield itself. A 4π active shielding can only partially reduce the problem of cosmic-ray background. An excellent solution is to install an accelerator facility in a laboratory deep underground [3]. As a pilot project, a 50 kV accelerator facility has been installed [4–6] in the Laboratori Nazionali del Gran Sasso (LNGS), where the flux of cosmic-ray muons is reduced by a factor 10^6 [7]. The Laboratory for Underground Nuclear Astrophysics (LUNA) pilot project was designed primarily for a renewed study of the ^{3}He(^{3}He,$2p$)^{4}He reaction ($Q = 12.86$ MeV) in the energy range of the solar Gamow peak ($E_0 \pm \delta E_0 = 21.9 \pm 6.2$ keV) for a central star temperature of $T = 15.5 \times 10^6$ K. The reaction is a member of the hydrogen burning proton-proton (pp) chain [2], which is predominantly responsible for the energy generation and neutrino luminosity [8] of the sun. So far, the reaction has been studied down to about 25 keV (Sec. II) but there remains the possibility of a narrow resonance at lower energies.

The hypothesis of a low-energy resonance was first advanced [9,10] as a solution to the solar neutrino puzzle, which in those days was regarded as a deficit of ^{8}B neutrinos. For this purpose a resonance with $E_R \simeq 21$ keV and $\Gamma < 6$ keV was considered [11] as the most favorable case. Experimental data available at that time were not inconsistent with

<u>57</u>   2700

the existence of a resonance with $E_R = 15$–20 keV and $\Gamma < 2$ keV [12]. As more data on solar neutrinos became available, it became clear that the deficit of ^{7}Be neutrinos is stronger than that of ^{8}B neutrinos. It was shown [12] that such a pattern of suppression occurs if $E_R \simeq 21$ keV.

Such a resonance level in ^{6}Be has been sought [2] without success by various indirect routes, and it is also not predicted by most nuclear-structure theories. However, the existence of this hypothetical resonance can be positively dismissed only by direct measurements at the required low energies (i.e., within the solar Gamow peak).

For nuclear reactions studied in the laboratory, the target nuclei and the projectiles are usually in the form of neutral atoms or molecules and ions, respectively. The electron clouds surrounding the interacting nuclides act as a screening potential: the projectile effectively sees a reduced Coulomb barrier. This in turn leads to a higher cross section $\sigma_s(E)$ than would be the case for bare nuclei, $\sigma_b(E)$ with an exponential enhancement factor [13,14]

$$f_{\text{lab}}(E) = \sigma_s(E)/\sigma_b(E) \simeq \exp(\pi\eta U_e/E), \qquad (2)$$

where U_e is the electron-screening potential energy (e.g., $U_e \simeq Z_1 \cdot Z_2 \cdot e^2/R_a$ approximately, with R_a an atomic radius). It should be pointed out that for a stellar plasma the value of $\sigma_b(E)$ must be known because the screening in the plasma can be quite different from that in laboratory studies [15], and $\sigma_b(E)$ must be explicitly included in each situation. Thus, a good understanding of electron-screening effects is needed to arrive at reliable $\sigma_b(E)$ data at low energies. Low-energy studies of several fusion reactions involving light nuclides showed [6,16,17] indeed the exponential enhancement of the cross section at low energies. The observed enhancement (i.e., the value of U_e) was, in all cases, close to or higher than the adiabatic limit derived from atomic-physics models. An exception is the previous ^{3}He $+$ ^{3}He data (Sec. II), which show apparently a flat $S(E)$ curve down to $E = 25$ keV, although the effects of electron screening should have enhanced the data at 25 keV by about a factor 1.2 for the adiabatic limit $U_e = 240$ eV. Thus, improved low-energy data are particularly desirable for this reaction.

We report here on such new data obtained by the LUNA Collaboration within the solar Gamow peak. Preliminary results, which have been published [18], are superseded by the present report.

II. THE ^{3}He(^{3}He,$2p$)^{4}He REACTION

The ^{3}He(^{3}He,$2p$)^{4}He reaction represents in the exit channel a three-body breakup: if the breakup is direct, one should observe a continuous energy distribution of the ejectiles described by phase-space considerations; if the breakup follows a sequential process, the energies of the ejectiles are described by two-body kinematics. Experiments have shown [19–21] that at energies below $E = 1$ MeV the reaction proceeds predominantly via a direct mechanism and that the angular distributions approach isotropy with decreasing energy. The $S(E)$ energy dependence observed by various groups [19–23] represents a consistent picture (Fig. 1). The only exception is the earliest experiment [24] where $S(E)$ is
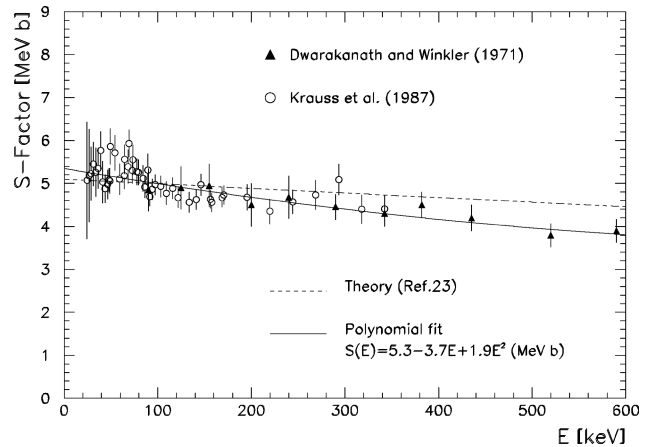

FIG. 1. Astrophysical $S(E)$ factor of the ^{3}He(^{3}He,$2p$)^{4}He reaction as obtained in previous work [20,21] (Sec. II). The solid curve is a polynomial fit to the data and the dotted curve a theoretical calculation [26] normalized to $S(0) = 5.1$ MeV b.

lower by a factor 3 to 5 compared to the other experiments; the discrepancy is most likely caused by target problems (^{3}He trapped in an Al foil).

The absolute $S(E)$ values of Refs. [20] and [21] (as well as those from the present work, Sec. VI) agree, at overlapping energy regimes, within experimental uncertainties, while those of Refs. [22] and [23] are lower by about 25%, suggesting a renormalization of their absolute scales. However, in view of the relatively few data points and their relatively large uncertainties, in comparison to the other data sets, it has been suggested [25] to omit these data, without significant loss of information. We verified that no changes in the $S(E)$ fit are appreciable (within 1%) by including or excluding the data sets from [22] and [23].

A reaction mechanism was suggested [26] at low energies, in which a neutron tunnels from one ^{3}He to the other, unimpeded by the Coulomb barrier, up to a radial distance where the nuclei overlap appreciably. In this model, a diproton remains and subsequently fissions into two protons. The calculated energy dependence of the $S(E)$ factor described well the data (dotted curve in Fig. 1), thus providing confidence in the extrapolation using a polynomial function (solid curve in Fig. 1):

$$S(E) = S(0) + S'(0)E + 0.5S''(0)E^2$$
$$= 5.3 - 3.7E + 1.9E^2 \ (\text{MeV b}). \qquad (3)$$

III. THE LUNA FACILITY

Technical details of the LUNA setup have been reported [5]. Briefly, the 50 kV accelerator facility (Fig. 2) consisted of a duoplasmatron ion source, an extraction and acceleration system, a double-focusing 90° analyzing magnet (with adjustable pole faces), a windowless gas-target system, and a beam calorimeter.

The energy spread of the ion source was less than 20 eV, the plasma potential energy deviated by less than 10 eV from the voltage applied to the anode, and the emittance of the source was 2 cm rad eV$^{1/2}$. The ion source provided a stable beam current of about 1 mA over periods of up to 4 weeks.
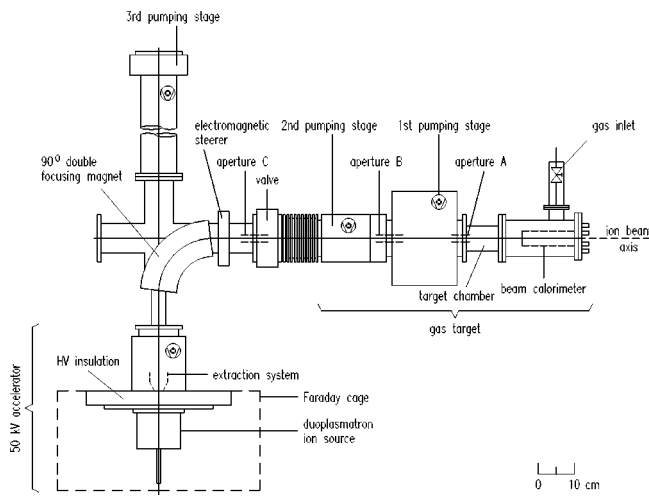
FIG. 2. Schematic diagram of the 50 kV LUNA accelerator facility (see also Figs. 2 and 3 of [5]).

The high voltage (HV) of the accelerator was provided by a power supply, which has a typical ripple of 5×10^{-5}, a longterm stability of better than 1×10^{-4}, and a temperature coefficient of better than $1.5 \times 10^{-4}/\text{K}$. The air-conditioned laboratory was kept at a temperature of $T = 21$ °C and a relative humidity of $H = 30\%$. The HV of the accelerator was measured with a resistor chain, contained in an air-tight plexiglass tube, and a digital multimeter. The resistor chain was built as a voltage divider, with fifty 20 MΩ resistors and one 100 kΩ resistor (temperature coefficient $= 1 \times 10^{-5}/\text{K}$). The multimeter (with a long term stability of 5×10^{-5} per year) provided the numerical value of the HV measured across the 100 kΩ resistor. This HV-measuring device was calibrated at the PTB in Braunschweig (Germany) at $T = (20 \pm 1)$ °C and $H = (35 \pm 10)\%$ to a precision of 5×10^{-5}.

The beam entered the target chamber of the differentially pumped gas-target system (three pumping stages) through apertures of high gas flow impedance (C to A in Fig. 2) and was stopped in the beam calorimeter. The gas pressure in the target chamber p_0 was measured with a Baratron capacitance manometer to an accuracy of better than 1%. This measurement was absolute and independent of the type of gas used. For ^{3}He gas (99.9% enriched in ^{3}He) of $p_0 = 0.50$ mbar pressure, the system reduced the pressure to 1×10^{-3}, 1×10^{-4}, and 1×10^{-5} mbar in the three upstream pumping stages; a similar pressure reduction was observed for other p_0 values. The gas composition in the target chamber was monitored with a mass spectrometer. The ^{3}He gas was compressed by Roots blowers, cleaned efficiently using a zeolite adsorption trap (cooled to liquid nitrogen temperature), and fed back into the target chamber (gas recirculation). The pressure p_0 was kept at a constant value using a needle valve in combination with an electronic regulation unit. As noted above, the main pressure drop occurred across the entrance aperture A (7 mm diameter, 40 mm length, 230 mm distance from aperture B). It was shown that the pressure in the target chamber was essentially unmodified by the gas flow through the entrance aperture A; thus, the geometrically extended target zone was characterized by a nearly static pressure. Beam-heating effects on the gas density are expected to be less than 0.5% [27] for a maximum $p_0 = 0.50$ mbar ^{3}He target pressure and the 500 μA maximum ^{3}He$^+$ beam current.

The beam current in the target area was determined to an accuracy of 3% using the beam calorimeter (with a constant temperature gradient). The calorimeter was placed (Fig. 3) at such a distance d from the center of aperture A ($d = 32.2 \pm 0.1$ cm) that angle straggling of the incident beam in the gas resulted in a beam profile smaller than the 200 mm^2 active area of the calorimeter.

The LUNA facility was equipped with an interlock system, which allowed the system to run without an operator on site. The duty time of the facility in the chosen running conditions was about 90%, with a weekly service time of 8 h. As the typical beam current in the target area was about 400 μA,
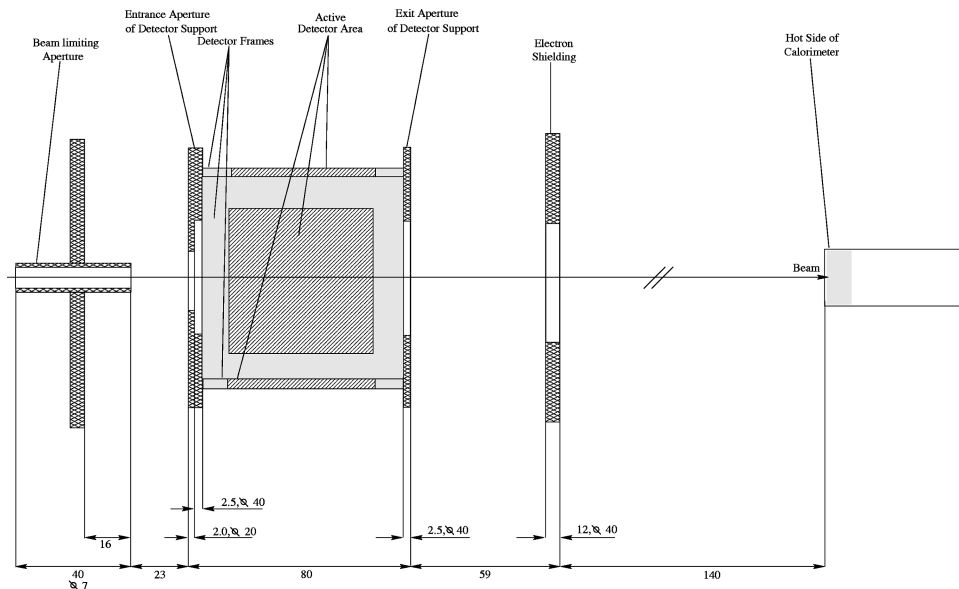

FIG. 3. Schematic diagram of the rectangular target chamber including the detection setup (telescopes) and the beam calorimeter; the given lengths and diameters (ϕ) are in units of mm (see also Figs. 4 and 5 in [5]).

a weekly charge of about 200 Cb could be accumulated on the target.

IV. THE DETECTION SETUP

The detection setup for the ^{3}He(^{3}He,$2p$)^{4}He studies had to fulfill the following requirements.

(1) A high absolute efficiency, in view of the expected reaction rates (yields) of about 1 event/day and less.

(2) A high rejection of natural radioactivity in the detectors, in the target chamber facing the detectors, and from the surrounding rocks at LNGS (mainly γ's); tests at LNGS have shown that commercial Si detectors exhibited an intrinsic radioactivity level, which was about 200 times higher than the above reaction yield.

(3) A high rejection of electronic noise, in view of the needed running times of several weeks per energy point.

(4) A clear separation of the reaction products from those of ^{3}He(d,p)^{4}He ($Q=18.35$ MeV), due to deuterium contamination in the ^{3}He beam (as HD$^+$ molecules of mass 3) and in the gas target (found to be smaller). This contaminant reaction has a cross section one millionfold higher than that of ^{3}He(^{3}He,$2p$)^{4}He at $E_{lab}=40$ keV, mainly due to the barrier ratio $E_c(d+^3$He$)/E_c(^3$He$+^3$He$)=0.56$, and thus extremely small deuterium contaminations (of order 10^{-7}) can lead to sizable event rates.

In order to optimize the detection setup and to understand the resulting spectra for quantitative analyses, a Monte Carlo program [28] was written to simulate the experiment under realistic conditions. The Monte Carlo program produces energy and time spectra of the ejectiles as well as absolute yields, which could be compared directly with data. Various quantitative tests of the Monte Carlo predictions have been carried out successfully [5,6,28]. A Monte Carlo simulation [28] of the proton spectrum from both reactions at a beam energy of 50 keV is shown in Fig. 4: a Ni foil of ^{3}He and ^{4}He stopping thickness (20 μm) was placed in front of a 1000 μm thick Si detector [maximum commercially available thickness at the time of the experimental project: the desirable thickness was 1400 μm to stop the 14.7 MeV protons from ^{3}He(d,p)^{4}He]; a deuterium contamination of 10^{-6} was assumed. One sees the continuous energy distribution of the protons from ^{3}He(^{3}He,$2p$)^{4}He and the peak(s) plus low-energy tail of protons from ^{3}He(d,p)^{4}He (due to incomplete stopping in the detector). Both proton spectra overlap appreciably leading to large uncertainties in the yield analysis of the ^{3}He(^{3}He,$2p$)^{4}He events; thus, the single spectra of Si detectors did not represent a viable solution. In addition, singles spectra would not reject the background due to natural radioactivity and electronic noise. By the requirement of proton-proton coincidences between detectors, placed on opposite sides of the beam axis, a unique signature of the ^{3}He(^{3}He,$2p$)^{4}He events could be obtained [21] in the coincidence spectra; also the background events (radioactivity and electronic noise) could essentially be eliminated. However, the price for this unique signature is a reduction of the absolute efficiency, by at least one order of magnitude compared to analysis via single spectra. Therefore, this approach was not followed; instead the present approach utilized ΔE-E detectors, in which single proton signals were detected in coincidence between the ΔE and E detectors of
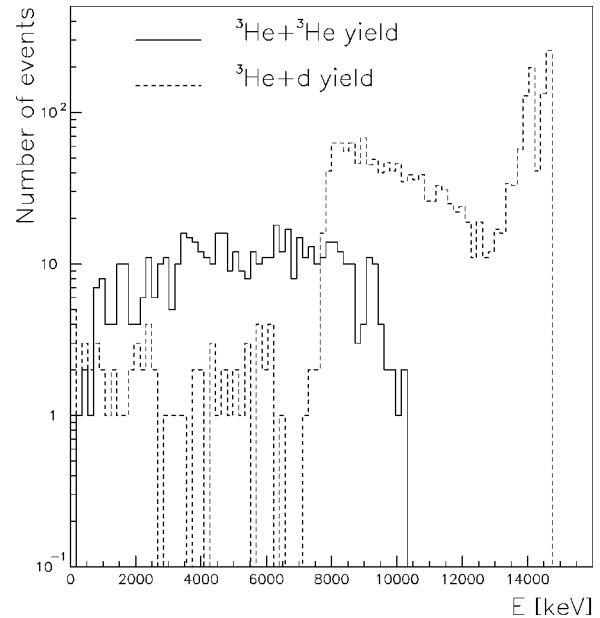

FIG. 4. Monte Carlo simulation of the protons from ^{3}He(^{3}He,$2p$)^{4}He and ^{3}He(d,p)^{4}He detected in a 1000 μm thick Si detector (covered with a 20 μm thick Al foil) at $E_{lab}=50$ keV and in the setup shown in Fig. 3. A deuterium contamination in the ^{3}He beam of $d/^3$He$=10^{-6}$ was assumed.

the telescope. In the detection setup (Fig. 3), designed according to the indications of Monte Carlo simulations, four ΔE-E telescopes (placed in a rectangular target chamber) were arranged around the beam axis: two opposite telescopes each at a distance of 2.7 cm from the beam axis and the two other telescopes each at 3.7 cm; the distance from the center of the entrance aperture A to the center in front of the telescopes was (8.3 ± 0.1) cm. The different distance from the center of the up-down and left-right couples of telescopes was due to mechanical constraints. Each telescope consisted of transmission surface barrier silicon detectors with a 0.25 μm thick Al layer deposited on both sides of the detectors. The ΔE and E detectors both had an active square area of 2500 mm^2; the ΔE (and E) detector had a thickness of 140 μm (and 1000 μm) and an energy resolution of 105 keV (and 55 keV) at $E_\alpha=5.5$ MeV. A Mylar foil (1.2 μm thick) and an Al foil (1.5 μm thick) were placed in front of each telescope; they stopped the intense elastic scattering yield and shielded the detectors from beam induced light. This double shielding was proved, in various background runs, to be effective and free from pinhole effects. The detectors were maintained permanently at low temperature (about -20 °C) using a liquid recirculating cooling system. The ^{4}He ejectiles from ^{3}He (^{3}He,$2p$)^{4}He ($E_\alpha=0$ to 4.3 MeV) and ^{3}He(d,p)^{4}He ($E_\alpha=3.7$ MeV) were stopped in the ΔE detectors, while the ejected protons from ^{3}He(^{3}He,$2p$)^{4}He ($E_p=0$ to 10.7 MeV) and ^{3}He(d,p)^{4}He ($E_p=14.9$ MeV) left signals in both the ΔE and E detectors of a given telescope (coincidence requirement). Figure 5 shows the identification matrix of one ΔE-E telescope simulated with the Monte Carlo program at $E_{lab}=50$ keV and assuming a deuterium contamination of 10^{-6}: the matrix reveals a clear separation of the events from both reactions.

Standard NIM electronics were used in connection with the four telescopes. The signals were handled and stored us-
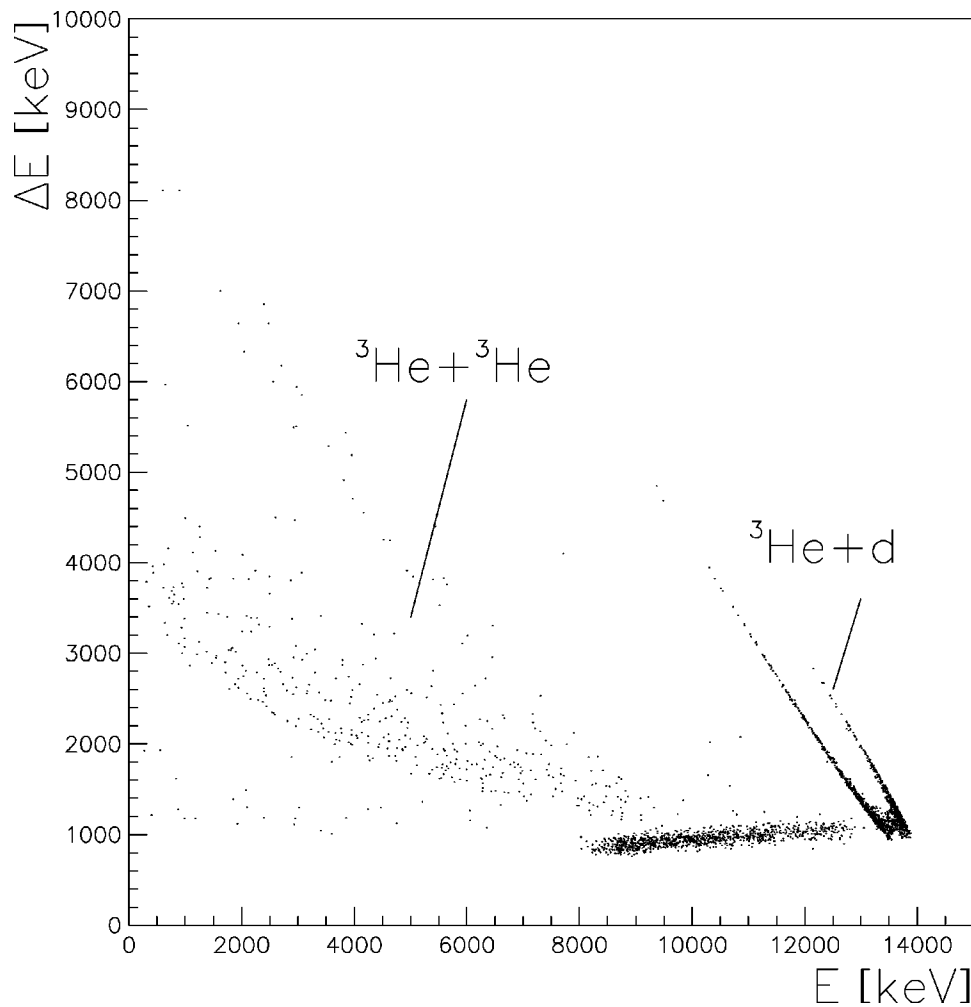
FIG. 5. Monte Carlo simulation of the ΔE-E identification matrix for the protons from $^{3}\text{He}(^{3}\text{He},2p)^{4}\text{He}$ and $^{3}\text{He}(d,p)^{4}\text{He}$ at $E_{\text{lab}}=50$ keV in the setup shown in Fig. 3. A deuterium contamination in the ^{3}He beam of $d/^{3}\text{He}=10^{-6}$ was assumed.

ing a CAMAC multiparametric system, which allowed for on-line as well as for play-back data analyses. Signals from two or more detectors were considered coincident within a time window of 1 μs, making negligible the rate of random coincidences. A pulser was permanently used in all detectors to check for dead time and electronic stability. The acquisition system also stored concurrent information on experimental parameters (such as ion beam current and charge, accelerator high voltage, and gas pressure in the target chamber) via CAMAC scalers. Controls were also implemented to stop data acquisition if the beam was lost or to reject an event if an error in the data transmission occurred. The system handles safely a data flux of about 500 events/s.

In the analysis of the data, the accepted events from $^{3}\text{He}(^{3}\text{He},2p)^{4}\text{He}$ had to fulfill the following three conditions.

(1) The events had to arise from proton-induced ΔE-E coincidences in a given telescope; the coincidence requirement of each telescope essentially eliminated events due to natural radioactivity of the detectors themselves and of surrounding materials.

(2) The events had to lie in a closed region of the ΔE-E plane (Fig. 6), whose borders were first deduced by Monte Carlo simulations and then fixed in order to cut the electronic noise.

(3) A proton event had to occur in only one given E detector, events which triggered more than one E-detector were rejected, this condition reduced significantly events due to the residual electronic noise, but it also rejected some p-p coincidences.

The chosen ΔE-E energy region together with the antico-incidence requirement led to an absolute detection efficiency of $(7.55\pm0.15)\%$ as determined by the Monte Carlo program. In the ΔE-E region of events from $^{3}\text{He}(^{3}\text{He},2p)^{4}\text{He}$ (Fig. 6), no background events were ever observed at LNGS since the installation of the equipment (January 1994) during several ''no beam'' and/or ''no target'' background measurements (up to two months running) as well as during a 10 day run with a ^{4}He beam and a ^{4}He target gas. At the Bochum laboratory (Earth surface) a background rate of about 10 events/day was found with the same setup. With the discussed operating conditions the setup sensitivity in terms of cross section values is better than 10^{-14} b. Although the selected regions in the spectra of the telescopes allow for a clear separation of the events from both reactions (Fig. 6), a few protons from the contaminant reaction $^{3}\text{He}(d,p)^{4}\text{He}$ can hit the detectors near the edges of their active volumes losing only a fraction of their energy and thus leading to a background rate in the ΔE-E region of the $^{3}\text{He}(^{3}\text{He},2p)^{4}\text{He}$
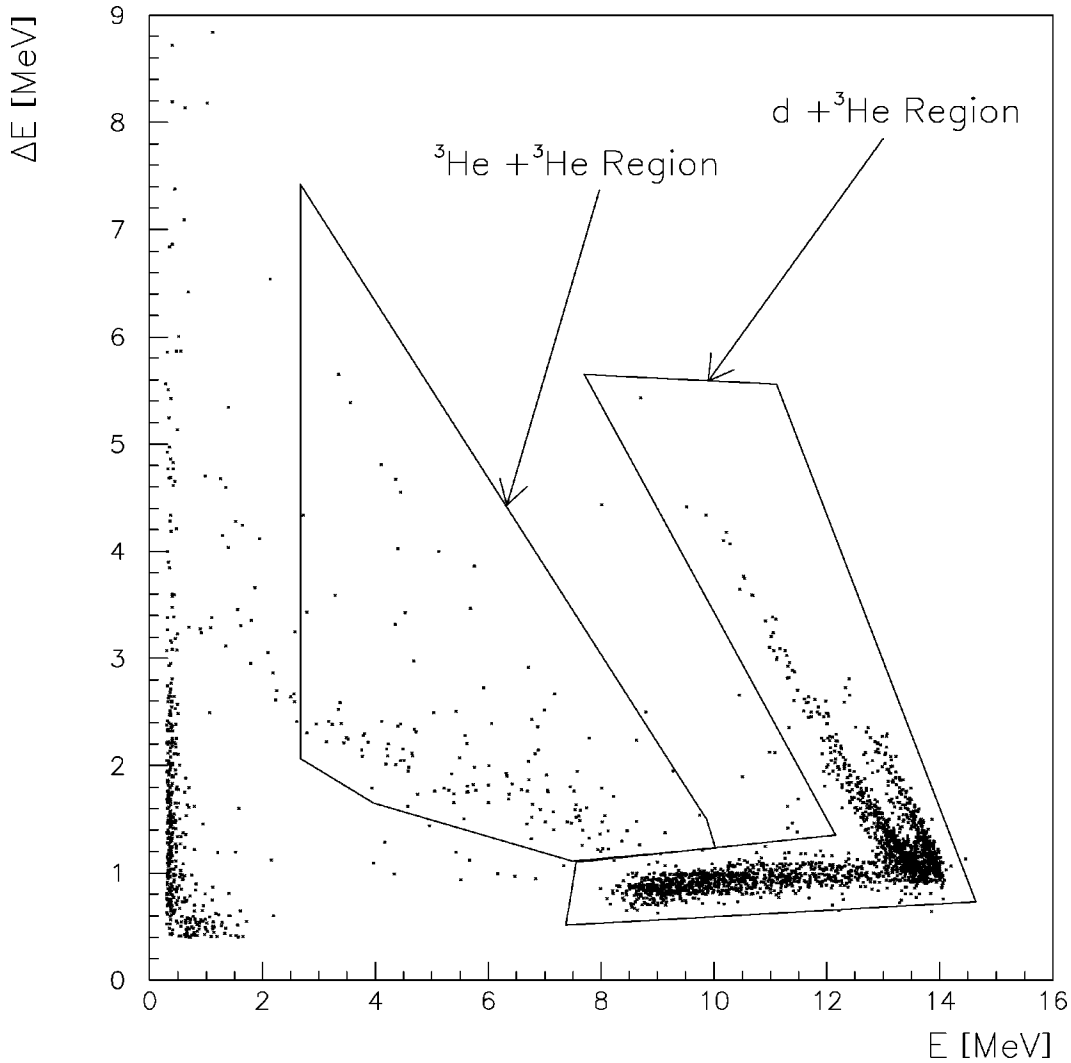
FIG. 6. ΔE-E identification matrix of one telescope (obtained in the setup of Fig. 3) at E_{lab}=50 keV and p_0=0.30 mbar. The ^{3}He+^{3}He and $d+^3$He selected regions are shown; note the beam-induced electronic noise at the left vertical edge of the matrix.

events. The probability of such events was investigated by the Monte Carlo program as well as by direct measurements using projectiles with Z/A=0.5 (selected by the 90° analyzing magnet). The ratio between the background events in the ^{3}He-^{3}He region and those in the clearly separated d-^{3}He region (=monitor) turned out to be (0.40±0.04)%. Thus a deuterium contamination equal to 10^{-7} allows $\sigma(E)$ measurements as low as E=15 keV, with a signal-to-background ratio equal to 4. During the reported experiments the deuterium contamination $d/^3$He ranged between 5×10^{-8} and 5×10^{-6}.

V. EFFECTIVE BEAM ENERGY AND ABSOLUTE CROSS SECTION

For the isotropic emission of the protons in ^{3}He(^{3}He,2p)^{4}He (Sec. II), the number of counts $dN(z)$ per unit of time arising from a differential length dz of the extended ^{3}He gas target is given by the expression

$$dN(z)=N_t N_b \sigma[E(z)]\eta(z)dz, \qquad (4)$$

where N_t is the ^{3}He target density in units of atoms/cm^3 (derived from the measured target pressure p_0, with a precision better than 1%), N_b is the number of ^{3}He projectiles per unit of time (derived from the beam calorimeter, with a precision of 3%), and $\eta(z)$ is the absolute detection efficiency of all four telescopes including geometry and the acceptance criteria discussed in Sec. IV. The efficiency also takes into account that two protons are produced per reaction. Introducing the stopping power ϵ (i.e., the energy loss per unit length), Eq. (4) can be rewritten in the form

$$dN(E)=N_t N_b \sigma(E)\eta(E)\epsilon(E)^{-1}dE. \qquad (5)$$

The total number of counts for the full target length L=(32.2±0.1) cm (from the center of the aperture A to the beam calorimeter) is then given by

$$N=N_t N_b \int_L \sigma(E)\eta(E)\epsilon(E)^{-1}dE. \qquad (6)$$

For the case of a thin target, i.e., introducing an effective

beam energy E_{eff} corresponding to the mean value of the projectile energy distribution in the detection setup (see below), one arrives at

$$N = N_t N_b \sigma(E_{\text{eff}}) \int_L \eta(E) \epsilon(E)^{-1} dE, \qquad (7)$$

where the values for E_{eff} and the integral were derived from the Monte Carlo program.

At sub-Coulomb energies a precise knowledge of the effective beam energy associated with observed yields is as important as the yield measurements themselves. For this reason, all Monte Carlo predictions have been thoroughly tested [28]. Here they are compared with a simple ''hand'' calculation. Let us consider the case of an incident ^{3}He energy of $E_{\text{lab}} = 50.00$ keV. The absolute energy is known to a precision of ± 2.5 eV, its long term stability is ± 5.0 eV, and the Gaussian energy spread [full width at half maximum (FWHM)] is 20 eV (Sec. III). When the beam passes through the gas target system filled with ^{3}He at the standard pressure of $p_0 = 0.30$ mbar, the beam loses energy in the three pumping stages and in the target chamber. For the calculation of this energy loss, we used stopping-power values given by the TRIM program [29]. It should be pointed out that experimental energy-loss data [30] at the relevant low energies were found to be consistent with those from the TRIM program, within the experimental error of 10%. We adopted this error in our analyses. With $\epsilon = (7.0 \pm 0.7)$ 10^{-15} eV/atom/cm^2 at $E_{\text{lab}} = 50$ keV one finds an energy loss of $\Delta E_1 = (2.2 \pm 0.2)$ eV in the three pumping stages and $\Delta E_2 = (430 \pm 43)$ eV over the (8.3 ± 0.1) cm distance from the center of aperture A to the center of the target chamber (detector location): $\Delta E_{\text{tot}} = (432 \pm 43)$ eV. The quoted error arises predominantly from the uncertainty in ϵ. This leads to an effective energy at the center of the target chamber of $E_{\text{lab}} = (49.568 \pm 0.043)$ keV. The telescopes see an effective target length of (7.0 ± 0.1) cm (see Fig. 7). The energy loss over this target length (i.e., the target thickness) is $\Delta E_3 = 365$ eV with an estimated error of ± 36 eV. For a constant $S(E)$ factor the cross section drops by 11.2% over this target thickness. Assuming a linear decrease in cross section over this region [2], the effective energy evaluation gives $E_{\text{lab}} = (49.572 \pm 0.045)$ keV, or a center-of-mass energy $E_{\text{eff}} = (24.786 \pm 0.023)$ keV. The error on E_{eff} transforms into a $\pm 1.5\%$ uncertainty on $\sigma(E_{\text{eff}})$. These estimates are consistent with Monte Carlo calculations simulating precisely the detection setup (Fig. 3) and the acceptance criteria of ^{3}He-^{3}He events. The effective energy, as deduced from the mean energy of the distribution shown in Fig. 8, correspond to $E_{\text{lab}**} = (49.568 \pm 0.043)$ keV. The spread of the energy distribution is determined by various effects: (a) the energy straggling [2,31] at the center of the target, $\delta_{E_1} = 125$ eV, (b) the thermal Doppler width [2] at room temperature, $\delta_{E_2} = 51$ eV, (c) the energy spread over the target length seen by the detectors, $\delta_{\Delta E_3} = 105$ eV. The total energy spread δ_E is therefore 171 eV, with an estimated error of ± 20 eV. This is in good agreement with the 189 eV spread predicted by the Monte Carlo program (Fig. 8). This procedure was applied for all beam energies and gas pressures. It should be noted that the 10% systematic uncertainty
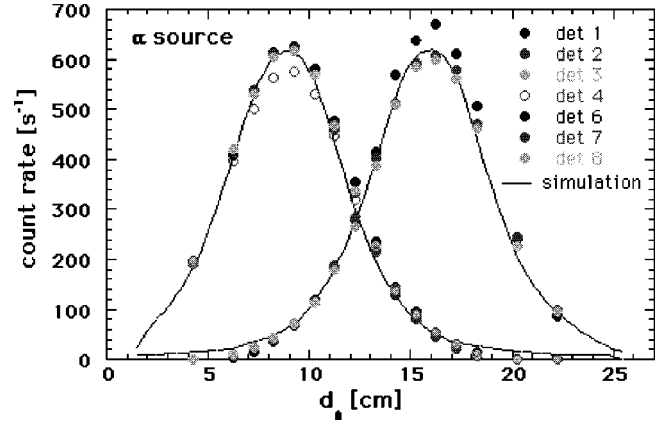

FIG. 7. Absolute detection efficiency in a new modified setup (to be used in future work) with eight E detectors (arranged in two consecutive boxes) as observed with an α source ($E_\alpha = 5.5$ MeV), which was moved along the beam axis (distance d_A measured from the center of the entrance aperture A). All the detectors have the same distance (2.7 cm) from the beam axis. The first section (four detectors) of the setup is nearly equivalent to the configuration in Fig. 3. The target length seen by one box (7 cm) is the same as in the setup in Fig. 3. The solid curves show the results of Monte Carlo simulations.

in the projectiles energy loss in the target induces only a 0.1 –0.2 % error on E_{eff} corresponding to a 1.0–3.5 % uncertainty in the $S(E)$ values.

From the geometry of the four square telescopes and the target length $L = 32.2$ cm one expects an absolute efficiency over this length of the order of 10%; the Monte Carlo simulations yield $(7.55 \pm 0.15)\%$. The geometrical setup efficiency was tested using an α source, which was moved along the beam axis. This test was possible, due to mechanical constraints, only recently with a new setup (to be used in future
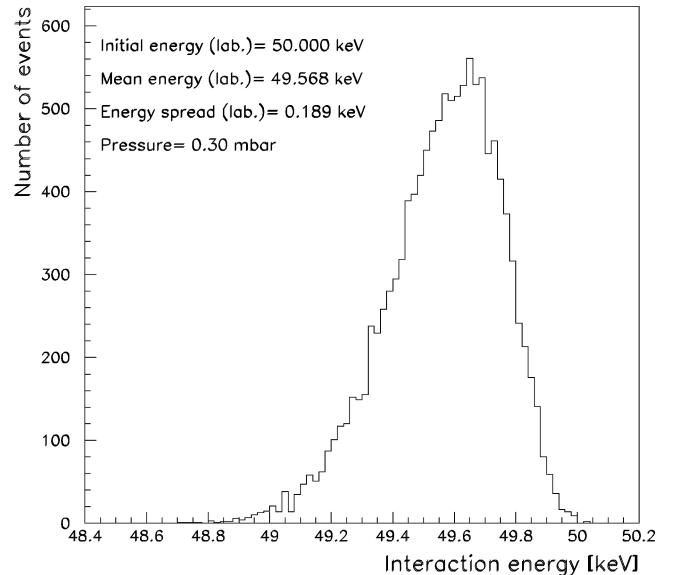

FIG. 8. Monte Carlo simulation of the energy distribution of the ^{3}He projectiles (incident energy $E_{\text{lab}} = 50.00$ keV, ^{3}He gas pressure $p_0 = 0.30$ mbar) leading to detected and accepted events in the setup of the four telescopes (Fig. 3). The mean energy of the distribution is $E_{\text{lab}**} = (49.568 \pm 0.043)$ keV and the energy spread is $\delta E = 189$ eV.

work) where eight 1000 μm thick detectors were placed in two consecutive boxes (each containing four detectors around the beam axis) all at the same distance from the beam axis. The results (Fig. 7) are in good agreement with the corresponding Monte Carlo simulations (solid curves in Fig. 7).

To test the reliability of the corrections applied in the data analyses, we performed measurements at $E_{lab}=50.00$ keV using different gas pressures, $p_0=0.15$, 0.30, and 0.50 mbar; for each pressure the target thickness, the energy loss, and the detection efficiency are different. The resulting $S(E)$ values (Table I) are fully compatible with each other, well inside the experimental uncertainties.

During another test period the detection setup was changed: the detector box was moved 5.0 cm closer to the beam calorimeter extending the total target length from 32.2 to 37.2 cm. The target pressure was fixed at $p_0=0.50$ mbar. In this setup a significant decrease (of the order of 25%) in reaction yield was predicted by the Monte Carlo simulations compared to the standard setup and standard pressure ($p_0=0.30$ mbar), due to the lower effective energy. The $S(E)$ results (Table I) are, within the experimental uncertainties, in good agreement with values deduced for the standard setup.

VI. RESULTS

Table I and Fig. 9 summarize the ^{3}He(^{3}He,$2p$)^{4}He results obtained until December 1996 with the LUNA setup at the 50 kV underground accelerator facility (LNGS). The lowest counting rate was 3 events per day at $E=20.76$ keV. The preliminary data [28] have been completely reanalyzed and have been integrated with the results of other new measurements. The data obtained at higher energies (450 kV accelerator in Bochum) with the LUNA setup [5] are also included for completeness. Previous literature data obtained at $E=24.51$ to 1080 keV [20,21] are also shown in Fig. 9. The LUNA data have been obtained at energies within the solar Gamow peak, i.e., below the 22 keV center of this peak, and represent the first measurement of an important fusion cross section at energies near the center of the Gamow peak. No evidence of the hypothetical resonance can be found in the covered energy range. The observed energy dependence $S(E)$, for bare nuclides $S_b(E)$ and shielded nuclides $S_s(E)$ was parametrized using the expressions [2,13]

$$S_b(E)=S_b(0)+S_b'(0)E+0.5S_b''(0)E^2, \qquad (8)$$

$$S_s(E)=S_b(E)\exp(\pi\eta U_e/E), \qquad (9)$$

where $S_b(0)$, $S_b'(0)$, $S_b''(0)$, and U_e are fit parameters. The data set shown in Fig. 9 was fitted, in the energy region between 20.7 and 1080 keV, using three methods.

(a) First $S_b(0)$, $S_b'(0)$, $S_b''(0)$ were obtained considering data for $E\geq100$ keV only, then U_e was deduced from all the data and the fixed $S_b(E)$ expression.

(b) All four parameters were allowed to change and the whole data set was fitted; the resulting curves for $S_b(E)$ and $S_s(E)$ are shown in Fig. 9 as dashed and solid curves, respectively.

TABLE I. $S(E)$ factor of ^{3}He(^{3}He,$2p$)^{4}He.

Energy[a] (keV)	Charge[b] (Cb)	Counts[c]	Background[d]	$S(E)$	ΔS_{stat}[h] (MeV b)	ΔS_{sys}[i]
91.70[f]	0.0373	16479	[e]	5.15	0.11	0.21
86.51[f]	0.0301	8931	[e]	5.23	0.11	0.22
81.50[f]	0.0544	8378	[e]	5.33	0.12	0.22
76.29[f]	0.209	22879	[e]	5.32	0.11	0.22
71.22[f]	0.0945	5012	[e]	5.43	0.14	0.26
66.06[f]	0.0615	2304	[e]	5.43	0.15	0.26
61.06[f]	0.238	3562	[e]	5.41	0.14	0.26
55.94[f]	0.257	2251	[e]	5.50	0.16	0.29
50.64[f]	0.825	2870	[e]	5.63	0.14	0.31
45.82[f]	0.784	1087	[e]	6.14	0.23	0.39
24.80[g,k]	204.2	128	14.5	5.96	0.62	0.23
24.70[g,j]	344.0	424	47.5	6.23	0.37	0.24
24.52[g,l]	49.5	100	7.7	7.10	0.79	0.31
24.30[g,m]	68.5	119	10.9	6.90	0.72	0.37
24.25[g,j]	99.8	93	5.0	6.66	0.74	0.26
23.70[g,j]	140.4	96	4.2	6.87	0.74	0.27
23.21[g,j]	122.9	73	8.2	7.50	1.02	0.30
23.15[g,m]	32.7	28	2.9	6.82	1.47	0.42
22.82[g,m]	139.3	103	12.5	7.21	0.84	0.39
22.78[g,j]	307.0	101	6.2	5.97	0.64	0.24
22.33[g,m]	113.9	57	3.7	7.27	1.05	0.40
22.28[g,j]	233.5	59	7.3	5.85	0.89	0.24
21.75[g,j]	373.9	77	2.4	7.63	0.91	0.31
21.23[g,j]	416.4	60	6.5	7.15	1.06	0.29
20.76[g,j]	1044.9	107	17.1	6.80	0.82	0.28

[a]Effective center-of-mass energy derived from the absolute energy of the ion beam and Monte Carlo calculations (including the energy loss of the projectiles in the target gas and the effects of the extended gas-target and detector geometries).

[b]Deduced from the beam calorimeter (3% accuracy).

[c]Observed events in the ^{3}He-^{3}He region (Fig. 4).

[d]Background events in the ^{3}He-^{3}He region equal to 0.40% of the observed counts in the d-^{3}He region of the spectra (Fig. 4), which must be subtracted from the counts in column 3.

[e]Negligible background.

[f]Data obtained with the LUNA setup at the 450 kV accelerator in Bochum [5], with the standard setup and target gas pressures ranging from 0.15 to 0.30 mbar.

[g]Data obtained with the LUNA setup and accelerator facility at LNGS (energy spread=20 eV); the chosen energy steps are of the order of the energy loss of the beam in the extended gas target.

[h]Statistical error (one standard deviation) including counting statistics and apparative variations [pressure (1%), beam power (1.3%), and temperature (1%)].

[i]Systematical error (one standard deviation) including uncertainties in pressure (1%), beam power (3%), efficiency (2%), beam energy (200 eV c.m. at Bochum, negligible at LNGS), and energy loss (10%).

[j]Target gas pressure equal to 0.30 mbar, standard detection setup position.

[k]Target gas pressure equal to 0.15 mbar, standard detection setup position.

[l]Target gas pressure equal to 0.50 mbar, standard detection setup position.

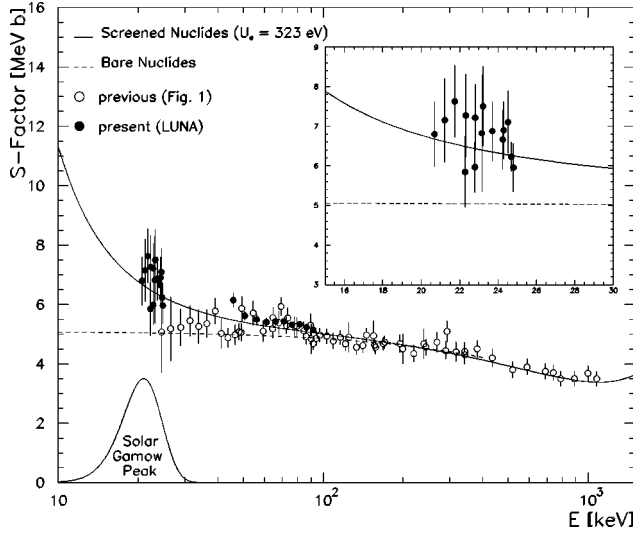[m]Target gas pressure equal to 0.50 mbar, modified detection setup position.

FIG. 9. The $S(E)$ factor of ^{3}He(^{3}He,2p)^{4}He from the previous work (Fig. 1) and the present work (Table I). The dashed and solid curves represent $S_b(E)$ and $S_s(E)$, respectively. The solar Gamow peak is shown in arbitrary units. The upper right corner inset zooms on the underground LUNA data.

(c) U_e was fixed at 240 eV (i.e., the value calculated in the adiabatic limit) while $S_b(0)$, $S_b'(0)$, and $S_b''(0)$ were allowed to vary.

The results are summarized in Table II. The three methods give compatible $S_b(E)$ values while U_e changes significantly: the methods (a) and (b) give U_e values higher than the adiabatic limit (240 eV), consistent with observations in other fusion reactions. It should be noted that by fitting the LUNA data only with method (b), a screening potential of 490±30 eV is obtained. The difference between observed and predicted U_e values is not understood at present. Therefore we adopted $S_b(0)$ from the theoretical adiabatic screening [method (c)] and derived a further error corresponding to the extreme cases U_e =0 eV [$S_b(0)$=5.7 MeV b] and U_e=432 eV [$S_b(0)$ =5.1 MeV b]:

$$S_b(0) = 5.40 \pm 0.05 \pm 0.30 \pm 0.30 \ \text{(MeV b)},$$

where the first two errors arise from statistical and systematical uncertainties, respectively, and the last error from the lack of understanding of electron screening.

TABLE II. $S_b(E)$ factor of ^{3}He(^{3}He,2p)^{4}He for bare nuclides and electron screening potential energy U_e, from different fitting procedures in the 20.7–1080 keV region. A description of the adopted procedures is given in the text.

$S_b(0)$ MeV b	$S_b'(0)$ b	$S_b''(0)$ b/MeV	U_e eV	χ^2	Method
5.1±0.1	−2.6±0.7	2.0±1.3	432±29	0.93	a
5.30±0.08	−3.6±0.6	3.8±1.1	323±51	0.85	b
5.40±0.05	−4.1±0.5	4.6±1.0	240	0.87	c

VII. A HYPOTHETICAL RESONANCE AT LOWER ENERGIES

The difference between the LUNA data in the 20.7–24.8 keV region and $S(E)$ calculated in the adiabatic limit (i.e., fixing U_e=240 eV), can be used to estimate upper limits for the strength of a hypothetical resonance located at lower energies. For each measured point we calculated an excess S factor $S_{\text{exc}}(E)$ from

$$S_{\text{exc}}(E) = S_{\text{meas}}(E) - S_{\text{ad}}(E), \quad (10)$$

where S_{meas}(E) are the data given in Table I corrected for a 240 eV screening potential and S_{ad} comes from the fit (c) in Table II, discussed above. The excess cross section, integrated in the measured energy interval (20.7–24.8 keV), gives the integral yield

$$Y_{\text{exc}} = (2.0 \pm 0.5) 10^{-15} \ \text{MeV b}. \quad (11)$$

We may compare this value with the tail of a low-energy resonance integrated over the same energy range. For this purpose, we adopted the following procedure: the resonant cross section $\sigma_{\text{res}}(E)$ was described according to the usual Breit-Wigner expression

$$\sigma_{\text{res}}(E) = \pi \lambdabar^2 \omega \Gamma_a(E) \Gamma_b(E) \frac{1}{(E-E_R)^2 + (\Gamma/2)^2}, \quad (12)$$

where $\lambdabar$ is the De Broglie wavelength, ω is the statistical factor, E_R is the resonance energy, and $\Gamma = \Gamma_a + \Gamma_b$ is the resonance total width. Due to the high energies of the protons in the exit channel, the partial width of the resonance decay $\Gamma_b(E)$ was assumed to be energy independent. For the partial width of the entrance channel $\Gamma_a(E)$ we used the expression [2]

$$\Gamma_{a,l}(E) = \left(\frac{2E}{\mu}\right)^{0.5} \frac{2\hbar}{R_n} P_l(E,R_n) \theta_l^2, \quad (13)$$

where μ=1.507 a.m.u. is the reduced mass, R_n=4 fm is the nuclear radius, and the dimensionless reduced width θ_l^2 of the nuclear state has an upper limit of unity ($\theta_l^2 \leq 1$, Wigner limit). The penetrability $P_l(E,R_n)$ is given by the equation

$$P_l(E,R_n) = \frac{1}{F_l^2(E,R_n) + G_l^2(E,R_n)}, \quad (14)$$

and was calculated for s waves (l=0) using the approximations for the Coulomb wave functions F_l and G_l given in [33]. It turns out that $\Gamma_a \ll 1$ keV at $E \leq 25$ keV (for θ_l^2=1) and thus $\Gamma \simeq \Gamma_b$.

Equations (12), (13), and (14) lead to the expression

$$\sigma_{\text{res}}(E) = A \frac{1}{E^{0.5}} \frac{1}{F_l^2(E,R_n) + G_l^2(E,R_n)} \frac{\Gamma}{(E-E_R)^2 + (\Gamma/2)^2}, \quad (15)$$

where the constant A contains the parameters μ, R_n, and θ_l^2. Its value can be determined by the comparison with the experimental value Y_{exc}:
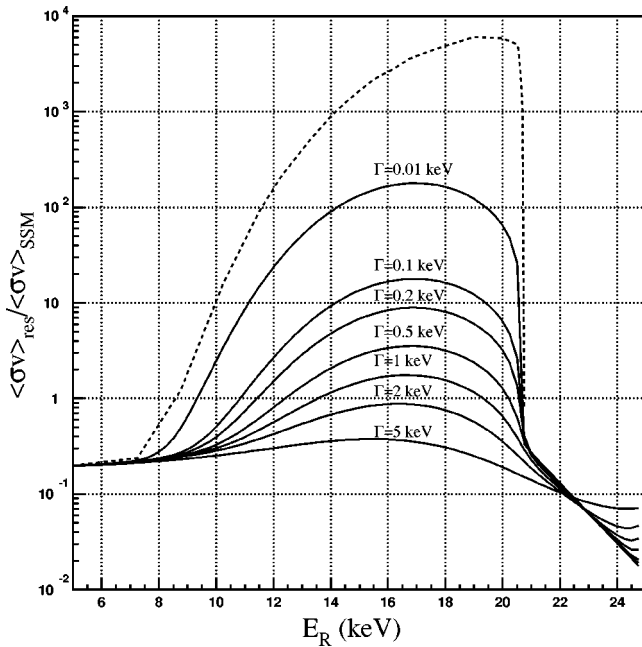
FIG. 10. The ratio $\langle\sigma v\rangle_{\mathrm{res}}/\langle\sigma v\rangle_{\mathrm{SSM}}$ of the resonance and non-resonance reaction as a function of the resonance energy E_R for some values of the total width Γ. The dashed curve shows the upper limit of this ratio considering the Wigner limit ($\theta_l^2 = 1$).

$$\int_{20.7}^{24.8} \sigma_{\mathrm{res}}(E)\,dE = Y_{\mathrm{exc}}. \qquad (16)$$

With this functional relation θ_l^2 is known for fixed values of the resonance energy E_R and of the total width Γ. It is then possible to evaluate the reaction rate $\langle\sigma v\rangle_{\mathrm{res}}$ of this hypothetical resonance and compare it with the nonresonant rate $\langle\sigma v\rangle_{\mathrm{SSM}}$ used in standard solar model (SSM) calculations. Figure 10 shows the calculated ratio $r = \langle\sigma v\rangle_{\mathrm{res}}/\langle\sigma v\rangle_{\mathrm{SSM}}$ as a function of E_R for some values of the total resonance width Γ, assuming a central temperature of the sun of 15×10^6 K. The dotted curve in Fig. 10 shows the reaction rate ratio in the Wigner limit ($\theta_l^2 = 1$), which was calculated using Eqs. (15) and (16).

The $\langle\sigma v\rangle_{\mathrm{res}}$ values obtained with this procedure are upper limits for the reaction rate due to the hypothetical resonance. At energies $E_R \lesssim 9$ keV one concludes that the presence of a resonance cannot account for even a partial nuclear solution of the solar neutrino puzzle [12,32]. The same conclusion applies in the energy region between 9 and 20 keV for resonance widths ≥ 2 keV. Room seems still available for a very narrow resonance in this interval where only direct measurements could rigorously dismiss (or confirm) its existence.

VIII. CONCLUSIONS

For the first time the ^{3}He(^{3}He,$2p$)^{4}He fusion reaction has been studied in an energy region deep inside the Gamow peak, i.e., down to 20.7 keV. This goal has been achieved at the new facility for nuclear astrophysics (LUNA) built in the underground laboratory of Gran Sasso (Italy). The results obtained so far show that the $S(E)$ energy dependence is consistent with the predictions based on an extrapolation from higher energies. The presence of a low-energy resonance in the ^{3}He(^{3}He,$2p$)^{4}He reaction, which could have strong effects on the "solar neutrino problem," does not emerge from the new data. In the near future the LUNA collaboration will extend the measurements down to $E = 17$ keV: the foreseen running time here is one year. Definite conclusions with respect to the expected solar neutrino fluxes have to await the results of these experiments. For this next phase a new detection setup, designed to reduce the background induced by deuterium contamination in the beam and in the gas target, has been developed and is now in the testing phase.

The electron screening effect, which produces an exponential enhancement of $S(E)$ at low energies, can be observed in the new ^{3}He(^{3}He,$2p$)^{4}He data. This is a second important result since previous data did not show a clear evidence of the enhancement (Fig. 1). The screening potential seems to be higher than the value predicted by the adiabatic model of the interaction between projectile and atomic electron clouds. It should be noted that the adiabatic approximation, among other electron screening models, is that giving the highest screening potential. A better quantitative determination of the screening potential will be possible when the LUNA Collaboration reaches the lowest energy scheduled for the ^{3}He(^{3}He,$2p$)^{4}He experiment. Hopefully, a complete and clear picture of the screening effect will be possible when data collected at very low energies and for other fusion reactions are available. This is one of the future goals of the LUNA Collaboration.

The excess of the screening potential could also be explained as a tail of a narrow resonance lying in the not measured low-energy region. Upper limits for the strength of such a resonance have been calculated assuming the adiabatic limit for the screening potential. Unfortunately, these calculations cannot exclude the existence of a narrow resonance (width <2 keV) at energies between 9 and 20 keV with a strength high enough to give a sizeable contribution to the ^{3}He(^{3}He,$2p$)^{4}He reaction rate in our Sun.

ACKNOWLEDGMENTS

[1] W. A. Fowler, Rev. Mod. Phys. **56**, 149 (1984).

[2] C. Rolfs and W. S. Rodney, *Cauldrons in the Cosmos* (University of Chicago Press, 1988).

[3] G. Fiorentini *et al.*, Z. Phys. A **350**, 289 (1995).

[4] C. Arpesella *et al.*, Report No. LNGS 91/18, 1991 (unpublished).

[5] U. Greife *et al.*, Nucl. Instrum. Methods Phys. Res. A **350**, 327 (1994).

[6] U. Greife *et al.*, Z. Phys. A **351**, 107 (1995).

[7] MACRO Collaboration, Phys. Lett. B **249**, 149 (1990).

[8] J. N. Bahcall and M. H. Pinsonneault, Rev. Mod. Phys. **64**, 885 (1992).

[9] W. A. Fowler, Nature (London) **238**, 24 (1972).

[10] V. N. Fetisov and Y. S. Kopysov, Phys. Lett. **40B**, 602 (1972).

[11] V. N. Fetisov and Y. S. Kopysov, Nucl. Phys. **A239**, 511 (1975).

[12] V. Castellani, S. Degl'Innocenti, and G. Fiorentini, Astron. Astrophys. **271**, 601 (1993).

[13] H. J. Assenbaum *et al.*, Z. Phys. A **327**, 461 (1987).

[14] L. Bracci *et al.*, Nucl. Phys. **A513**, 316 (1990).

[15] B. Ricci *et al.*, Phys. Rev. C **52**, 1095 (1995).

[16] P. Prati *et al.*, Z. Phys. A **350**, 171 (1994).

[17] K. Langanke *et al.*, Phys. Lett. B **369**, 211 (1996).

[18] C. Arpesella *et al.*, Phys. Lett. B **389**, 452 (1996).

[19] A. D. Bacher and T. A. Tombrello, Rev. Mod. Phys. **37**, 433 (1965).

[20] M. R. Dwarakanath and H. Winkler, Phys. Rev. C **4**, 1532 (1971).

[21] A. Krauss *et al.*, Nucl. Phys. **A467**, 273 (1987).

[22] M. R. Dwarakanath, Phys. Rev. C **9**, 805 (1974).

[23] N. M. Wang *et al.*, Sov. J. Nucl. Phys. **3**, 777 (1966).

[24] W. M. Good *et al.*, Phys. Rev. **83**, 845 (1951).

[25] E. Adelberger *et al.*, *Workshop on ''Solar fusion rates,''* Seattle, 1997 (unpublished).

[26] R. May and D. D. Clayton, Astrophys. J. **153**, 855 (1968).

[27] J. Goerres *et al.*, Nucl. Instrum. Methods Phys. Res. A **241**, 334 (1985).

[28] C. Arpesella *et al.*, Nucl. Instrum. Methods Phys. Res. A **360**, 607 (1995).

[29] J. F. Ziegler, Program TRIM-95, IBM Research, 1995.

[30] R. Golser and D. Semrad, Nucl. Instrum. Methods Phys. Res. B **69**, 18 (1992).

[31] F. Besenbacher *et al.*, Dan. Vid. Selsk. **40**, 1 (1981).

[32] V. Berezinsky, G. Fiorentini, and M. Lissia, Phys. Lett. B **365**, 185 (1996).

[33] M. Abramowitz and J. A. Stegun, *Handbook of Mathematical Functions* (GPO, New York, 1965).